



Comparative evaluation of packed-bed performance of biomass ashes as adsorbents for removal of diuron from aqueous solution

Sunil K. Deokar^a, Sachin A. Mandavgane^{a,*}, Bhaskar D. Kulkarni^b

^aDepartment of Chemical Engineering, Visvesvaraya National Institute of Technology, South Ambazari Road, Nagpur 440010, India, Tel. +91 712 2801650; email: sunildeokar.2008@gmail.com (S.K. Deokar), Tel. +91 712 2801563; Fax: +91 712 2223969; emails: sam@che.vnit.ac.in, mandavgane1@gmail.com (S.A. Mandavgane)

^bCSIR-National Chemical Laboratory, Dr. HomiBhabha Road, Pune 411008, India, Tel. +91 20 25902770, ext. 2772; Fax: +91 20 25902612; email: bd.kulkarni@ncl.res.in

Received 11 December 2015; Accepted 19 May 2016

ABSTRACT

The packed-bed performance of biomass ashes (BMA), namely rice husk ash (RHA) and bagasse fly ash (BFA), was investigated for adsorptive removal of diuron (herbicide) under dynamic conditions. The effects of influent concentration (10–30 mg/L), flow rate (1–3 mL/min), and bed height (3–11 cm) were studied at 30°C and results were analyzed using various packed-bed models. The saturation time and capacity of the BFA bed were found to be approximately 1.5 and 1.6 times higher due to higher BET surface area than that of RHA bed. However, the bed utilization of RHA was higher because of smaller mass transfer zone. At a constant influent concentration (20 mg/L) and flow rate (1 mL/min), the maximum volume of diuron treated was 1,325 and 1,685 mL using RHA (bed height 10 cm) and BFA (bed height 11 cm), respectively. Among the packed-bed models applied, the BDST model revealed the inconsistent MTZ and complex mechanism involving more than one rate-controlling step for the adsorption of diuron on both ashes. The kinetics in the initial part of the breakthrough curve was governed by external mass transfer according to the Bohart–Adams and Wolborska models. Better agreements between experimental and predicted values of bed capacities for each ash and the higher bed capacity of BFA than RHA were demonstrated by the Thomas model. The Yoon–Nelson model was found to be superior for BFA rather than for RHA to estimate 50% saturation time. However, the deactivation kinetic model, previously discovered and applied only for gas–solid adsorption, was found to be the best for the diuron–BMA (liquid–solid) adsorption system in this study.

Keywords: Diuron; Biomass ashes; Rice husk ash; Bagasse fly ash; Packed-bed model

1. Introduction

Diuron [3-(3,4-(dichlorophenyl)-1,1 dimethylurea)] is a nonselective pre- and post-emergent urea herbicide, and is applied globally to control the growth of

broadleaf and grassy weeds in both agricultural and nonagricultural sites [1,2]. However, large amounts of the herbicide sprayed on the field accidentally leaches into soil and eventually into the soil ecosystem, where it either degrades or remains in its original form for a longer period [3,4]. Diuron has a mean half-life of about 330 d in soil [5]. It has high chemical stability

*Corresponding author.

together with high leaching potential. Its presence is detected in both surface water and ground water in different zones worldwide [6]. According to a European Union regulation, the maximum permissible concentration of an herbicide in drinking water is $0.1 \mu\text{g/L}$ [7]. Several techniques which have been proposed to alleviate the environmental risk of leached herbicides, such as diuron are adsorption, biological methods, advanced oxidation processes, and hydrodechlorination [8]. Adsorption, one of the most widely used and established methods for pollutant removal from water [9], is effectively implemented for batch removal of diuron using potent adsorbents such as activated carbon, polymers, carbon nanotubes, soils, and clays [6–8,10–13]. However, the performance of these adsorbents for continuous removal of diuron in packed bed has not yet been evaluated. Continuous adsorption in packed-bed column is commercially worth evaluating because the constant contact between the adsorbate and the adsorbent allows for efficient utilization of the adsorbent, thus producing better quality effluent [14,15].

In a previous work [16], we studied the behavior of low-cost, easily available biomass ashes (BMAs), especially rice husk ash (RHA) and bagasse fly ash (BFA) for batch adsorption of diuron. It was observed that BFA has higher adsorption potential due to its higher surface area and greater carbon content than RHA. We also found increased adsorption of diuron on bigger particles of BMA (RHA and BFA) due to greater carbon-to-silica ratio and surface area. The adsorption capacity (m^2/g) of BMA was found to be comparable with that of activated carbon/fiber and greater than that of soils, wheat carbon, clay minerals, and nanotubes. Although our batch adsorption experiment suggested that BMA is both cost-effective and efficient, its performance needs to be evaluated for continuous process.

In this work, we have investigated and compared the packed-bed parameters of RHA and BFA for continuous removal of diuron using the packed-bed column technique. The effects of influent concentration, flow rate, and bed height on adsorption are studied and the results are analyzed for various packed-bed models. In addition to the conventional packed-bed model, the deactivation kinetic model, which was originally developed for gas–solid adsorption system, was applied for diuron–BMA (liquid–solid) adsorption.

2. Materials and methods

2.1. Adsorbents

RHA was obtained from M/s Yash Agro Ltd, Nagpur (India) and BFA from M/s Wainganga Sugar

and Power Ltd. Bhandara (India). Rice husk and bagasse were used as solid fuels to fire the boilers in these industries. Proximate analysis of each ash was performed according to an Indian Standard method for testing coal and coke samples [17]. The surface area, pore diameter, and volume were measured using the BET surface area analyzer (ASAP 2010; Micromeritics, Germany). The chemical composition of both ashes was investigated using XRF analysis (PW 2403; PANalytical, Netherlands). The percentage of carbon, hydrogen, nitrogen, and sulfur in BMA were determined with the CHNS technique using an elemental analyzer (vario MACRO Cube; Elementar, Germany).

2.2. Adsorbate

The adsorbate diuron (98%) was purchased from Sigma Aldrich and used without any treatment. The chemical formula and molecular weight of diuron are $\text{C}_9\text{H}_{10}\text{Cl}_2\text{N}_2\text{O}$ and 233 (g/mol), respectively. The stock solution of diuron was prepared in deionized water and the solution was diluted successively for different experimental runs.

2.3. Experimental method

2.3.1. Packed-bed adsorption study

A glass column of 0.9 cm internal diameter and 30 cm height was fabricated for continuous removal of diuron in packed bed. The glass column had four alternate openings at different positions from the bottom to collect the effluent. According to the desired height of the bed, the adsorbent (g) was packed between two supporting layers of glass wool. The glass wool was used to avoid the loss of adsorbent during the flow of effluent. The deionized (about 50 mL) water was pumped upward through the bed using a peristaltic pump (PP201 V; Electro Lab, India), and this allowed to remove entrapped air in the adsorbent bed. Prior to diuron adsorption, the column was kept inactive overnight. The constant influent rate of diuron solution was maintained by mounting a rotameter between the pump and the column. The samples were collected from the outlet periodically and the effluent concentration (C_t , mg/L) was measured on a UV–vis spectrophotometer (Model UV 1800; Shimadzu, Japan) at 248 nm. The column experiments were performed at a constant temperature ($30 \pm 2^\circ\text{C}$) and pH (6.5) for different influent concentrations (C_0), flow rates (Q), and bed heights (Z), according to the experimental conditions presented in Table 1. Average value of duplicate experiments was reported. Results were plotted in the form

Table 1
Experimental conditions

Expt. no.	Influent concentration C_0 (mg/L)		Flow rate Q (mL/min)		Bed height Z (cm)	
	RHA	BFA	RHA	BFA	RHA	BFA
	E1	10	10	1	1	6
E2	20	20	1	1	6	7.5
E3	30	30	1	1	6	7.5
E4	20	20	1	1	6	7.5
E5	20	20	2	2	6	7.5
E6	20	20	3	3	6	7.5
E7	20	20	1	1	3	4
E8	20	20	1	1	6	7.5
E9	20	20	1	1	10	11

breakthrough (BT) curves (C_t/C_0 vs. time) for each experiment. The breakthrough (t_b or $t_{0.1}$) and saturation (t_s) points were assumed at $C_t/C_0 = 0.10$ and $C_t/C_0 = 0.97$ on BT curves, respectively.

2.4. Determination of packed-bed parameter

The dynamics of column are usually studied by evaluating the column parameters for different conditions. The column parameters that directly decide the feasibility and economics of adsorption are the bed capacity at breakthrough time and at saturation time, length of the mass transfer zone (MTZ), fractional bed utilization (FBU), and percentage of removal. The capacity at breakthrough point (q_b mg/g) and capacity at saturation (q_s mg/g) point were calculated as follows [15]:

$$q_b = \frac{C_0 Q}{m} \int_0^{t_b} \left(1 - \frac{C_t}{C_0}\right) dt \quad (1)$$

$$q_s = \frac{C_0 Q}{m} \int_0^{t_s} \left(1 - \frac{C_t}{C_0}\right) dt \quad (2)$$

where m (g) is the mass of adsorbent. The percentage removal was determined from the quantity (mg) of diuron added and adsorbed in column. The length of bed used for adsorption is known as the “mass transfer zone” (MTZ; cm) [15], which was obtained using Eq. (3):

$$MTZ = Z \left(1 - \frac{q_b}{q_s}\right) \quad (3)$$

The bed at the start of MTZ is 100% saturated; at this point, the adsorbate concentration is equal to the influent concentration. By contrast, the bed at the end of MTZ is 0% saturated; at this point, the adsorbate concentration is zero. The MTZ is useful for determining the FBU. The empty bed contact time (EBCT) also called “residence time,” influences the volume of adsorbate treated and nature of BT curve. The EBCT (min) and adsorbent usage rate, U_r (g/mL), were calculated using Eqs. (4) and (5), respectively [18]:

$$EBCT = \frac{V_C}{Q} = \frac{A_C Z}{Q} \quad (4)$$

$$U_r = \frac{m}{V_b} = \frac{V_C \rho}{V_C N_b} \quad (5)$$

where V_C (m^3) is the volume of adsorbent in bed, A_C (m^2) is the cross-sectional area of column, V_b (m^3) is the volume of solution treated at breakthrough, ρ (g/cm^3) is the apparent density of adsorbent, and N_b is the number of bed volumes of solution to breakthrough.

3. Results and discussion

3.1. Characterization of BMA

Results of proximate analysis indicated the following composition: 1.80% moisture, 6.16% volatile matter, 89.87% ash, and 2.14% fixed carbon in RHA; and 6.30% moisture, 42.46% volatile matter, 40.16% ash, and 11.10% fixed carbon in BFA. The carbon percentage determined using CHNS analysis of RHA and BFA was 5.85 and 47.37, respectively, whereas the silica content investigated by XRF analysis was 81.78 and 36.14%, respectively. In addition, RHA/BFA

contains 4.08/1.10% Al_2O_3 , 1.87/2.32% K_2O , 1.27/1.62% Fe_2O_3 , 1.27/3.10% CaO , 0.50/1.86% MgO , 0.19/1.20% Na_2O , 0.78/3.05% P_2O_5 , 0.12/1.15% MnO , 0.40/1.22% TiO_2 , 0.008/0.12% CuO , respectively. The composition of BMA depends on combustion techniques (moving grate, fluidized bed, and suspension/entrained combustion chamber), geographical location of cultivation of crops and process conditions (efficiency). The metal oxides develop charges on ash surface depending on solution pH when the ash is added to the aqueous solution. This enables faster adsorption of ionic species on the BMA surface. The BET surface area of RHA and BFA was found to be 34 and $52 \text{ m}^2/\text{g}$, indicating the dominant proportion of carbon over silica in providing higher surface area for BFA. The density of RHA having an average particle size of $144 \mu\text{m}$ was found to be $258 \text{ kg}/\text{m}^3$, whereas that of BFA having an average particle size of $118 \mu\text{m}$ was found to be $212 \text{ kg}/\text{m}^3$. The micropore area of RHA was $6 \text{ m}^2/\text{g}$, whereas that of BFA was $14 \text{ m}^2/\text{g}$. The external surface area was determined using the BET surface area and micropore area and was found to be 28 and $38 \text{ m}^2/\text{g}$ for RHA and BFA, respectively. The pore volume and pore diameter of RHA and BFA were 2.69×10^{-3} and $4.96 \times 10^{-2} \text{ cm}^3/\text{g}$ and 81 and 46 \AA , respectively. The measurement of pore volume and pore diameter indicates the presence of shallower pores on the RHA surface and deeper pores on the BFA surface. This can be verified from scanning electron micrographs (SEMs) of RHA and BFA. The SEM images presented in Fig. 1 reveal the shallower and bigger diameter pores on the RHA surface, and deeper and smaller diameter pores on the BFA surface. The interconnected and elongated pores in BFA and reptured pores in RHA can also be observed in these figures. The BFA surface looks more porous than RHA.

The FTIR spectra of RHA and BFA before and after adsorption of diuron are shown in Fig. 2. In the

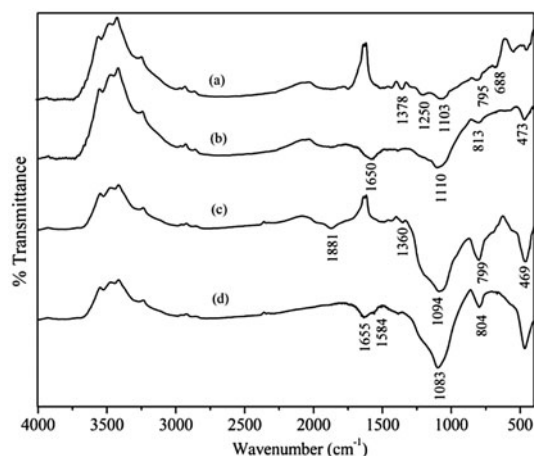


Fig. 2. FTIR spectra of blank BFA (a), BFA after adsorption of diuron (b), blank RHA (c) and RHA after adsorption of diuron (d).

spectra of blank RHA and BFA (i.e. before adsorption), the band at $1,667\text{--}2,000 \text{ cm}^{-1}$ indicates the weak combinations and overtone absorption. The peaks in this region may be attributed to the mono- to hexasubstitution of aromatic ring [19]. The bands between $1,360$ and $1,380 \text{ cm}^{-1}$ are ascribed to the aromatic C–H and carboxyl–carbonate structures [19]. The peaks at $1,103$ and 795 cm^{-1} in BFA and at $1,094$ and 799 cm^{-1} in RHA are due to asymmetric and symmetric stretching vibrations of Si–O–Si, respectively [20,21]. The stretching vibrations of Si–O at 688 cm^{-1} may be characteristic of quartz in BFA [22]. The peak at 469 cm^{-1} in RHA may be due to the presence of Si–H bond; the asymmetric stretching of internal tetrahedral SiO_4 group in BFA is indicated by a band at $1,250 \text{ cm}^{-1}$ [19]. After adsorption of diuron, the new peaks at $1,650 \text{ cm}^{-1}$ (Fig. 2, spectrum b) in BFA and at $1,655 \text{ cm}^{-1}$ (Fig. 2, spectrum d) in RHA

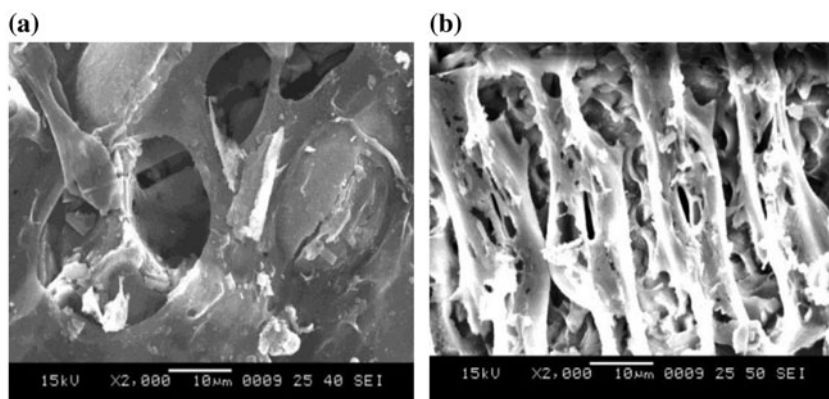


Fig. 1. SEMs of (a) RHA and (b) BFA.

appeared. These could be attributed to the presence of C=O in diuron [23]. A weak stretching of the C–C bond in diuron is indicated by a weak peak at 1,584 (cm^{-1}) in RHA spectra after adsorption of diuron [23]. In addition, the shifting of the peaks after adsorption of diuron can be observed in both RHA and BFA spectra.

3.2. Packed-bed parameters

The packed-bed parameters in Table 2 for RHA and BFA show that EBCT is inversely proportional to flow rate and directly proportional to bed height at a constant adsorbent dosage and flow rate, respectively. The adsorbent usage rate, that is, the mass of adsorbent saturated/volume of solution treated, is reduced with increase in EBCT. The bed capacities (q_b and q_s) of BFA are greater than that of RHA. In Table 2, it can be observed that the difference between q_b and q_s of each experiment for BFA is greater than that for RHA. This indicates the presence of more number of unoccupied adsorption sites after breakthrough in BFA. The exhaustion of BFA bed was slow, compared with RHA. Therefore, the volume (V_e) of diuron solution treated using BFA was larger. In Table 2, the increment in MTZ indicates the decrease in FBU. The length of MTZ is more in BFA than in RHA, whereas the FBU is more in RHA than in BFA. Thus, it can be

suggested that higher the length of MTZ, lesser the utilization of adsorbent bed. The percentage removal of diuron on RHA and BFA is nearly same. It can be observed that the saturation time of BFA bed is approximately 1.5 times higher than that of RHA bed and the capacity at saturation of BFA is about 1.6 times greater than that of RHA under the experimental conditions studied.

In a previous study [16], the batch adsorption capacities of RHA and BFA were observed to be 2.3 and 9.8 (mg/g), respectively. In this study, the packed-bed adsorption capacities of RHA and BFA were 4.13 and 6.77 (mg/g), respectively. The packed-bed capacity of RHA is higher than that in batch, whereas it is the reverse for BFA. This may be due to the dominating effect of concentration gradient at the solid–liquid interface in the RHA–diuron system. The interaction time between BFA and diuron in packed bed may be insufficient, thus resulting in the early discharge of diuron molecules. As a result, the bed capacity is reduced.

3.3. Effect of process parameters

3.3.1. Effect of influent concentration

The influent concentration is changed, according to the experimental conditions in Table 2, at constant

Table 2
Comparison of packed-bed parameters of RHA and BFA for diuron adsorption under different conditions

C_0	Q	Z	EBCT	t_b	t_s	V_e	N_b	U_r	q_b	q_s	MTZ	FBU	Removal %
<i>RHA</i>													
10	1	6	3.82	365.43	870.45	870.45	47.03	0.005	1.56	2.83	2.69	0.55	65.04
20	1	6	3.82	180.50	619.63	619.63	23.26	0.011	1.78	3.49	2.94	0.51	56.37
30	1	6	3.82	110.08	492.58	492.58	14.24	0.018	1.98	4.13	3.12	0.48	50.17
20	1	6	3.82	180.50	619.63	619.63	23.26	0.011	1.78	3.49	2.94	0.51	56.37
20	2	6	1.91	71.55	395.67	791.35	18.44	0.014	1.40	3.02	3.22	0.46	38.11
20	3	6	1.27	30.56	234.66	703.97	11.81	0.022	0.90	2.87	4.13	0.31	40.27
20	1	3	1.91	88.01	346.55	346.55	21.39	0.012	1.42	3.12	1.63	0.46	44.97
20	1	6	3.82	180.50	619.63	619.63	23.26	0.011	1.78	3.49	2.94	0.51	56.37
20	1	10	6.36	427.45	1,324.57	1,324.57	31.47	0.008	2.42	3.92	3.83	0.62	51.77
<i>BFA</i>													
10	1	7.5	4.77	452.98	1,305.87	1,305.87	58.36	0.004	2.21	4.25	3.60	0.52	65.05
20	1	7.5	4.77	271.50	1,055.64	1,055.64	34.98	0.007	2.72	5.67	3.90	0.48	53.74
30	1	7.5	4.77	207.10	935.47	935.47	26.68	0.010	3.02	6.77	4.15	0.45	48.24
20	1	7.5	4.77	271.50	1,055.64	1,055.64	34.98	0.007	2.72	5.67	3.90	0.48	53.74
20	2	7.5	2.38	115.58	520.73	1,041.47	29.78	0.009	2.40	5.31	4.11	0.45	50.03
20	3	7.5	1.59	57.79	285.07	855.22	22.34	0.012	1.94	4.92	4.55	0.39	44.58
20	1	4.0	2.54	114.47	391.93	391.93	29.50	0.009	2.25	4.57	2.03	0.49	58.30
20	1	7.5	4.77	271.50	1,055.64	1,055.64	34.98	0.007	2.71	5.67	3.92	0.48	53.74
20	1	11.0	6.99	510.91	1,685.48	1,685.48	43.89	0.006	3.43	6.04	4.76	0.57	53.77

flow rate and bed height for RHA and BFA. The results obtained, which are illustrated in the form of BT curves in Fig. 3, indicate the early saturation of each BMA, as only limited adsorption sites are available for higher influent concentration. This leads to a reduction in breakthrough and saturation times (Table 2), thus, resulting in steeper BT curves at higher influent concentration. Besides, the activation energy at higher concentration is enhanced due to surface coverage of RHA and BFA, which makes further adsorption difficult [18]. However, the gradient at higher influent concentration offers a greater driving force for mass transfer, and consequently the bed capacities (q_b and q_s) are improved at higher concentrations. The capacity at breakthrough is enhanced by about 1.3 times, whereas capacity at saturation point is enhanced by about 1.5 times (Table 2) for each ash when the influent concentration is increased by 3 times. The slow approach of BT curves (i.e. tailing) during the column saturation stage is ascribed to the control of intraparticle diffusion over the mass transfer process [24]. The growth in MTZ is higher for the BFA bed due to increased bed capacity than for RHA. The usage rate of BFA (U_r) per milliliter of diuron solution is enhanced by 2.5 times, whereas that of RHA is enhanced by 3.6 times when the influent concentration is augmented by 3 times. Compared with RHA, the BFA usage rate is less due to the higher surface area (i.e. adsorption sites).

3.3.2. Effect of flow rate

The effect of flow rate on adsorption of diuron was studied at a constant influent concentration and bed height by varying the flow rate (Table 1). The increase in flow rate from 1 to 3 (mL/min)

corresponds to the residence time of diuron from 3.82 to 1.27 (min) with RHA and from 4.77 to 1.59 (min) with BFA. It seems that the reduction in residence time at a higher flow rate adversely affected the breakthrough and saturation times as well as the bed capacities and percentage removal (Table 2). The diminution in capacity (q_b or q_s) and percentage removal for higher flow rate is attributed to insufficient contact time, resulting in early discharge of diuron molecules from the BMA bed before the equilibrium point is achieved. Similar results have been previously reported by Sadaf et al. [25] in packed-bed adsorption of dye. In comparison with BFA, the decrease in breakthrough and saturation times is more for RHA owing to lower EBCT. The lower flow rate offers adequate time for diuron molecules to penetrate into BMA pores, resulting in extended BT curves as shown in Fig. 4. From Table 2, it can be understood that the saturation of BFA bed is 1.7 times slower than that of RHA at 1 (mL/min) flow rate. The length of MTZ is increased but FBU is decreased due to increased mass transfer with flow rate. Han et al. reported the similar change in length of MTZ with respect to variable flow rate [24].

3.3.3. Effect of bed height

Fig. 5 shows the BT curves for adsorption of diuron on RHA and BFA at different bed heights for 20 (mg/L) influent concentration and 1 (mL/min) flow rate. As the bed height (i.e. adsorbent loading) is increased, the surface area, and therefore, the adsorption sites are also increased. Hence, the bed capacities (Table 2) of RHA and BFA are enhanced for higher bed height. Moreover, the BT curves are significantly extended as a result of greater saturation and

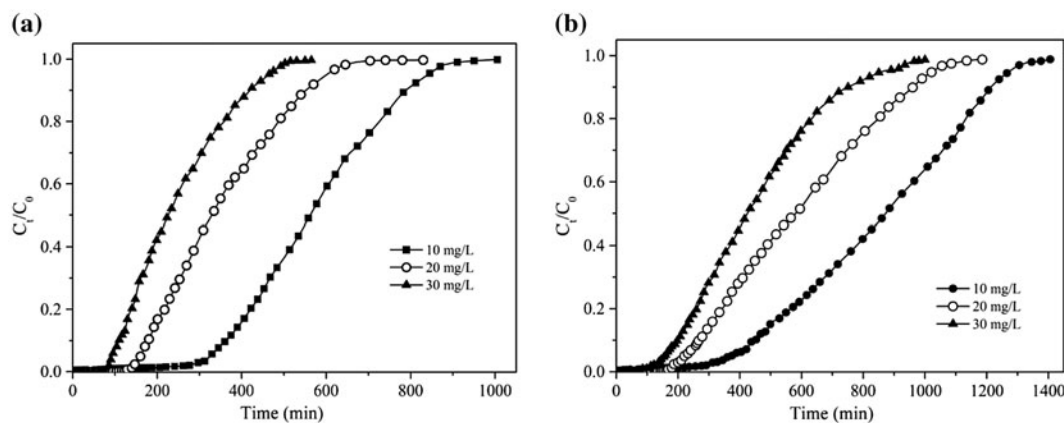


Fig. 3. Breakthrough curves for diuron removal in packed bed of (a) RHA ($Q = 1$ mL/min, $Z = 6$ cm) and (b) BFA ($Q = 1$ mL/min, $Z = 7.5$ cm) at different influent concentrations.

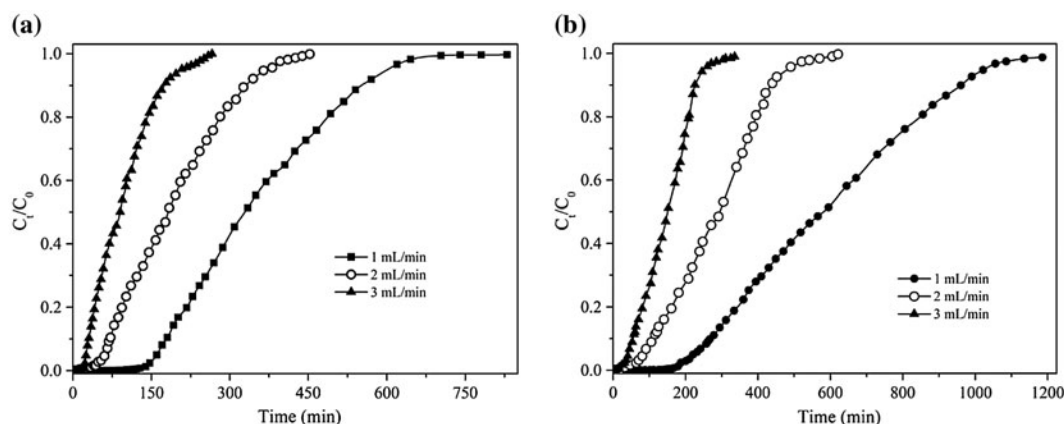


Fig. 4. Breakthrough curves for diuron removal in packed bed of (a) RHA ($C_0 = 20$ mg/L, $Z = 6$ cm) and (b) BFA ($C_0 = 20$ mg/L, $Z = 7.5$ cm) at different flow rates.

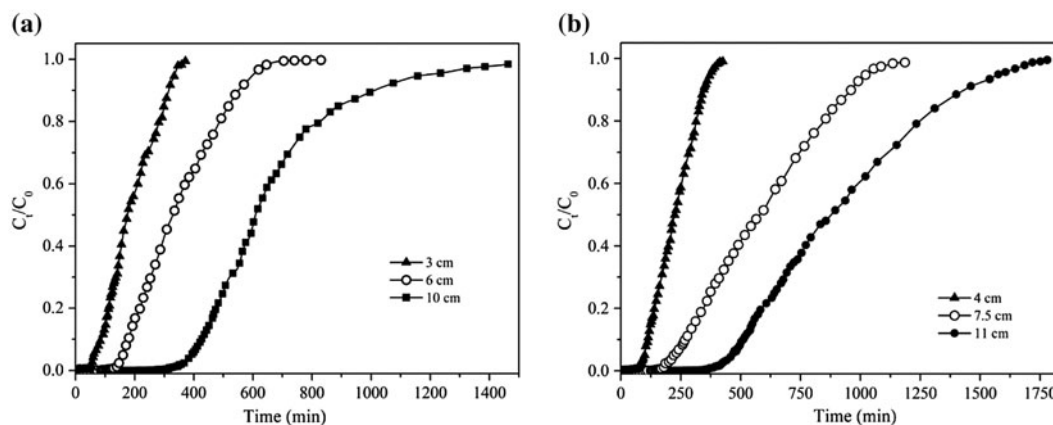


Fig. 5. Breakthrough curves for diuron removal in packed bed of (a) RHA ($C_0 = 20$ mg/L, $Q = 1$ mL/min) and (b) BFA ($C_0 = 20$ mg/L, $Q = 1$ mL/min) at different bed heights.

breakthrough times for both ashes. The increase in the breakthrough and saturation times could be ascribed to the longer distance it takes for the MTZ to move from the entrance of the bed to the exit when the bed height is increased [26]. The expansion of MTZ, similar to that in this study, was also reported by Pilli et al. [27]. The volume of solution treated using BFA is considerably higher than that using RHA for the same loading of each ash (1–3 g). However, bed utilization of RHA is more due to smaller MTZ. The growth in capacity at saturation point of each ash is nearly 1.3 times for a threefold increase in ash dosage, but the capacity at breakthrough point is enhanced by approximately 1.5 times. This indicates the fast uptake of diuron until breakthrough, which slows down slightly after breakthrough due to lower concentration gradient.

3.4. Application of packed-bed models

The few packed-bed models developed for solid–liquid adsorption systems are bed depth service time, Bohart–Adams, Wolborska, Thomas, Clark, and Yoon–Nelson models [14]. In addition to these, the deactivation kinetic model, which was initially derived for gas–solid adsorption is also applied in this study (solid–liquid adsorption).

3.4.1. Application of the Bed Depth Service Time model

The BDST model, Eq. (6), is based on the assumption that the adsorption is controlled by surface reaction between adsorbate and unused capacity of adsorbent [28]. The model considers the negligible intraparticle diffusion and external mass transfer resistance.

$$t = \frac{N_0}{C_0 U_0} Z - \frac{1}{C_0 K_{BD}} \ln \left(\frac{C_0}{C_t} - 1 \right) \quad (6)$$

where U_0 (cm/min) is a linear flow velocity. Here, the model is applied for 10, 50, and 90% BT at variable bed height and at constant concentration and flow rate. The BDST model (t vs. Z) is shown in Fig. 6 for packed-bed adsorption of diuron on RHA and BFA.

The adsorption capacity, N_0 (mg/L), is calculated from slope and found to be 1,473, 1,981, and 3,052 for RHA, and 1,781, 3,012, and 4,992 for BFA at 10, 50, and 90% BT, respectively. The bed capacity (90% BT) of BFA predicted by the BDST model is about 1.5-fold greater than that of RHA. The rate constant, K_{BD} (L/(mg min)), determined from intercept is 1.5×10^{-3} for RHA and 8.9×10^{-4} for BFA at 10% BT of column. The values of coefficient of determination (R^2) shown in Fig. 6 are close to one indicating the fitting of the BDST model for experimental data obtained for both ashes. However, R^2 values for 90% BT are slightly lesser than for 10 and 50% BT. This is due to the intraparticle diffusion in the final stage of bed saturation, leading to uneven variation in 90% BT with change in bed height. The linear lines in Fig. 6 for 10, 50, and 90% BT are not parallel, which is indicative of different lengths of MTZ. Therefore, it can be suggested that the MTZ does not move with constant velocity during packed-bed adsorption of diuron on RHA and BFA. This is because the bed height is not enough to have a fully developed profile, which is called a “constant pattern behavior” [26]. Ideally, the linear line corresponding to 50% BT should pass through the origin; but in present investigation, the 50% BT lines for RHA and BFA were intercepting the Y-axis. Therefore, according to the BDST model, adsorption of diuron on

each ash is governed by a complex mechanism involving more than one rate-controlling step [18].

3.4.2. Application of the Bohart–Adams and Wolborska models

The Bohart–Adams and Wolborska models are previously applied to investigate the behavior of column in the initial part of BT curve [29]. Therefore, in this study, these models were considered for the data in the range between 0% and 60% BT (i.e. $C_t/C_0 = 0-0.6$). The linear forms of Bohart–Adams and Wolborska models are given by the Eqs. (7) and (8), respectively. The BT curves predicted by these models are compared with experimental curves in Figs. 7a and 7b for adsorption of diuron on RHA and BFA, respectively.

$$\ln \left(\frac{C_t}{C_0} \right) = K_{AB} C_0 t - K_{AB} N_0 \left(\frac{Z}{U_0} \right) \quad (7)$$

$$\ln \frac{C_t}{C_0} = \frac{\beta C_0}{N_0} t - \frac{\beta Z}{U_0} \quad (8)$$

where K_{AB} (L/(mg min)) and β (min^{-1}) are the kinetic constants for the Bohart–Adams and Wolborska models, respectively, and N_0 (mg/L) is the adsorption capacity. The values of kinetic constants and adsorption capacity for RHA and BFA are given in Table 3a. Diuron adsorption capacities— N_0 (mg/L) for the Bohart–Adams model and Q_W (mg/g) ($=N_0/\text{density of BMA}$) for the Wolborska model—are directly proportional to concentration and bed height, and are inversely proportional to flow rate. The gradient at

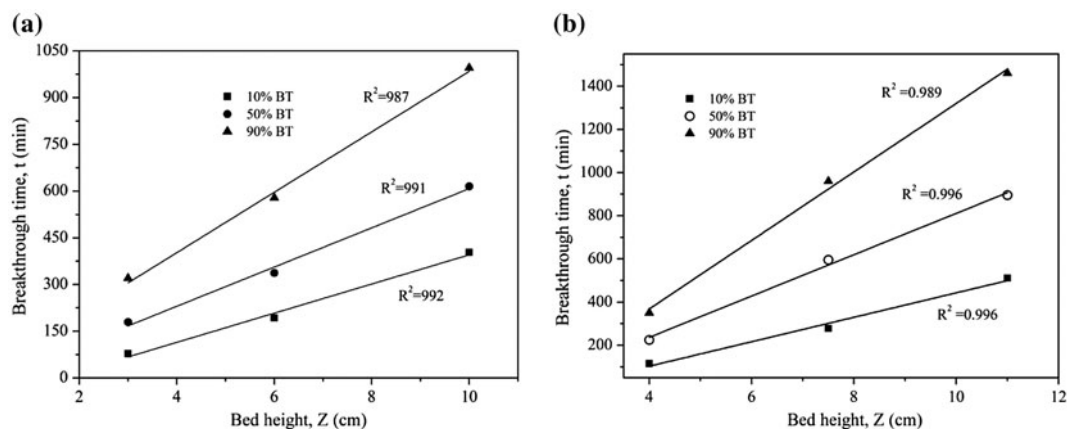


Fig. 6. Bed Depth Service Time model for adsorption of diuron on (a) RHA and (b) BFA at different bed heights ($C_0 = 20$ mg/L, $Q = 1$ mL/min).

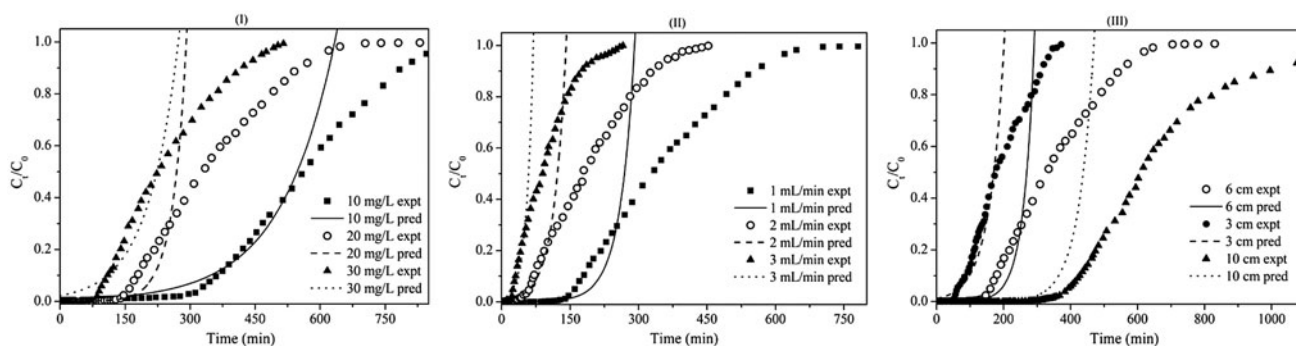


Fig. 7a. Comparison between experimental and predicted breakthrough curves for packed bed adsorption of diuron on RHA using Bohart–Adams and Wolborska models (I) $Q = 1$ mL/min, $Z = 6$ cm; (II) $C_0 = 20$ mg/L, $Z = 6$ cm; (III) $C_0 = 20$ mg/L, $Q = 1$ mL/min.

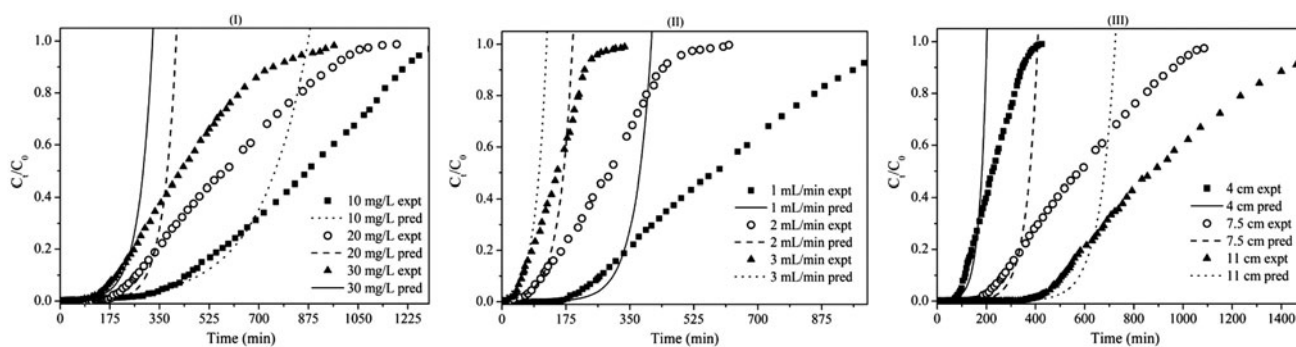


Fig. 7b. Comparison between experimental and predicted breakthrough curves for packed bed adsorption of diuron on BFA using Bohart–Adams and Wolborska models (I) $Q = 1$ mL/min, $Z = 7.5$ cm; (II) $C_0 = 20$ mg/L, $Z = 7.5$ cm; (III) $C_0 = 20$ mg/L, $Q = 1$ mL/min.

higher concentration and surface area for larger bed height are responsible for higher capacity. The higher flow rate causes insufficient residence time for diffusion; therefore, both N_0 and Q_W decrease with flow rate. The deviation between experimental and predicted values of (C_t/C_0) was calculated using Marquardt's percent standard deviation (MPSD) and that of between experimental and predicted t_b using percentage deviation (ϵ) [18,30]. The MPSD values in Table 3a are comparatively smaller for adsorption on BFA than for adsorption on RHA, which indicates the better fitting of the Bohart–Adams and Wolborska models for adsorption of diuron on BFA. Because the Bohart–Adams model is based on the control of external mass transfer on adsorption rate, the fitting of this model for the diuron–BMA system indicates that the overall system kinetics is dominated by external mass transfer in the initial part of adsorption in the column [31].

3.4.3. Application of Thomas models

The Thomas model is used for the data in a range of $0.01 < (C_t/C_0) < 0.97$ to determine maximum solid-phase concentration of diuron and adsorption rate on RHA and BFA. The linear form of the Thomas model is expressed by Eq. (9):

$$\ln\left(\frac{C_0}{C_t} - 1\right) = \frac{K_T q_0 m}{Q} - K_T C_0 t \quad (9)$$

The values of adsorption capacity q_0 (mg/g) and kinetic constant K_T [L/(mg min)] presented in Table 3a are the function of concentration, flow rate, and bed height. Chen et al. has previously reported similar changes in Thomas model capacity and kinetic constant with variation in concentration, flow rate, and bed height [31]. It is due to the driving force created by concentration difference. The MPSD values for

Table 3a
Parameters of packed bed models for adsorption of diuron on RHA and BFA

Expt no.	Bohart–Adams model				Wolborska model				Thomas model							
	K_{AB} (L/(mg min))	N_0 (mg/L)	t_b pred (min)	ϵ	MPSD	β (min ⁻¹)	Q_w (mg/g)	t_b pred (min)	ϵ	MPSD	K_T (L/(mg min))	q_0 (mg/g)	t_b pred (min)	ϵ	MPSD	
	<i>RHA</i>															
E1	1.50×10^{-3}	1,662.47	346.43	5.20	80.10	2.57	6.45	346.43	5.20	80.10	1.08×10^{-3}	2.80	355.63	2.68	30.86	
E2	0.80×10^{-3}	1,713.19	250.05	-38.53	77.36	1.33	6.65	250.05	-38.53	77.36	0.75×10^{-3}	3.53	206.99	-14.67	39.57	
E3	0.47×10^{-3}	2,143.92	108.17	1.73	61.03	1.00	8.32	108.17	1.73	61.03	0.47×10^{-3}	3.78	95.20	13.52	41.72	
E4	0.80×10^{-3}	1,713.19	250.05	-38.53	77.36	1.33	6.65	250.05	-38.53	77.36	0.75×10^{-3}	3.84	206.99	-14.67	39.57	
E5	2.00×10^{-3}	1,376.11	73.69	-2.99	56.21	2.75	5.34	73.69	-2.99	56.21	0.95×10^{-3}	3.50	59.57	16.74	46.77	
E6	3.30×10^{-3}	1,096.12	34.81	-13.90	65.48	3.62	4.25	34.81	-13.90	65.48	1.45×10^{-3}	3.03	25.34	17.09	40.45	
E7	1.30×10^{-3}	1,633.59	67.25	23.59	58.73	2.12	6.34	67.25	23.59	58.73	1.45×10^{-3}	3.56	101.99	-15.89	36.20	
E8	0.80×10^{-3}	1,713.19	250.05	-38.53	77.36	1.33	6.65	250.05	-38.53	77.36	0.75×10^{-3}	3.84	206.99	-14.67	39.57	
E9	0.68×10^{-3}	1,979.85	501.52	-17.33	75.48	1.78	7.68	501.52	-17.33	75.48	0.55×10^{-3}	4.02	503.07	-17.69	41.40	
	<i>BFA</i>															
E1	7.00×10^{-4}	1,502.60	387.63	14.43	47.05	1.05	6.79	387.63	14.43	47.05	6.12×10^{-4}	4.41	516.30	-13.98	17.56	
E2	1.10×10^{-3}	1,717.39	304.84	-12.28	54.68	1.89	7.76	304.84	-12.28	54.67	3.53×10^{-4}	6.15	300.97	-10.85	22.49	
E3	7.00×10^{-4}	2,046.30	215.64	-4.12	44.28	1.43	9.25	215.64	-4.12	44.28	2.67×10^{-4}	7.07	196.72	5.01	20.30	
E4	1.10×10^{-3}	1,717.39	304.84	-12.28	54.68	1.89	7.76	304.84	-12.28	54.67	3.53×10^{-4}	6.15	300.97	-10.85	22.49	
E5	1.35×10^{-3}	1,641.51	110.42	4.46	61.8	2.22	7.42	110.42	4.46	61.80	8.03×10^{-4}	5.56	140.49	-21.55	21.91	
E6	1.70×10^{-3}	1,536.43	54.39	5.88	89.27	2.61	6.94	54.39	5.88	89.26	1.45×10^{-3}	4.47	73.20	-26.66	24.08	
E7	1.75×10^{-3}	1,587.53	136.10	-18.89	55.86	2.78	7.17	136.10	-18.89	55.86	1.20×10^{-3}	4.56	136.45	-19.20	28.85	
E8	1.10×10^{-3}	1,717.39	304.84	-12.28	54.68	1.89	7.76	304.84	-12.28	54.67	3.53×10^{-4}	6.15	300.97	-10.85	22.49	
E9	8.00×10^{-4}	2,071.31	580.46	-13.61	65.49	1.66	9.36	580.46	-13.61	65.48	2.51×10^{-4}	6.74	571.36	-11.83	35.94	

Table 3b
Parameters of packed bed models for adsorption of diuron on RHA and BFA

Expt. no.	Yoon–Nelson model					Clark model					Deactivation kinetic model				
	K_{YN} (min^{-1})	$t_{0.5}$ expt (min)	$t_{0.5}$ pred (min)	ϵ	MPSD	A	r (min^{-1})	t_b pred (min)	ϵ	MPSD	k_0 ($\text{mL}/(\text{g min})$)	k_d (min^{-1})	t_b pred (min)	ϵ	MPSD
<i>RHA</i>															
E1	0.010	557.75	603.80	-8.26	29.53	3.70×10^{12}	0.028	455.32	-230.85	134.12	1.806	0.007	363.36	0.57	21.54
E2	0.016	334.48	372.69	-11.42	40.60	1.06×10^{18}	0.047	525.93	-462.68	115.56	1.495	0.010	180.40	0.05	11.57
E3	0.013	204.50	253.69	-24.05	24.32	1.28×10^{10}	0.107	120.18	-69.26	107.56	1.339	0.012	101.37	7.91	9.021
E4	0.016	334.48	372.69	-11.42	40.60	1.06×10^{18}	0.047	525.93	-462.68	115.56	1.495	0.010	180.40	0.05	11.57
E5	0.019	241.91	194.47	19.61	23.98	1.57×10^8	0.053	46.21	30.67	173.46	2.564	0.015	70.75	1.11	15.83
E6	0.028	125.23	95.25	23.94	31.64	0.28×10^7	0.068	-14.82	149.86	117.14	3.561	0.028	23.47	23.20	15.52
E7	0.021	220.95	191.90	13.15	33.21	6.51×10^{14}	0.071	48.72	3.57	128.68	1.114	0.016	82.08	6.73	9.94
E8	0.016	334.48	372.69	-11.42	40.60	1.06×10^{18}	0.047	525.93	-462.68	115.56	1.495	0.010	180.40	0.05	11.57
E9	0.015	617.23	647.80	-4.95	37.39	4.90×10^8	0.041	433.63	-255.20	101.48	2.703	0.007	423.35	0.96	19.10
<i>BFA</i>															
E1	0.007	885.45	847.86	4.25	21.76	10.02×10^6	0.010	852.20	-88.13	75.25	1.565	0.004	471.29	-4.04	23.48
E2	0.008	595.254	570.38	4.18	20.42	28.01×10^3	0.013	203.23	25.15	71.66	1.424	0.005	282.92	-4.21	11.31
E3	0.009	434.2	435.18	-0.22	25.55	7.55×10^3	0.017	78.29	62.20	79.00	1.368	0.007	199.01	3.91	8.72
E4	0.008	595.254	570.38	4.18	20.42	28.01×10^3	0.013	203.23	25.15	71.66	1.424	0.005	282.92	-4.21	11.31
E5	0.014	297.5	301.36	-1.30	21.22	14.63×10^3	0.023	86.65	25.03	93.80	2.725	0.010	121.57	-5.18	6.80
E6	0.026	152.383	152.69	-0.20	12.64	8.91×10^3	0.041	36.49	36.86	73.63	4.000	0.019	63.41	-9.72	9.34
E7	0.021	224.74	234.62	-4.40	27.87	11.13×10^3	0.024	167.58	-46.40	105.70	0.802	0.013	111.34	2.73	18.88
E8	0.008	595.254	570.38	4.18	20.42	28.01×10^3	0.013	203.23	25.15	71.66	1.424	0.005	282.92	-4.21	11.31
E9	0.006	895.05	935.17	-4.48	32.01	95.55×10^4	0.010	617.20	-20.80	107.70	3.119	0.004	496.43	2.83	15.21

the Thomas model in Table 3a for RHA and BFA indicate better agreement between experimental and predicted (C_t/C_0) values; therefore, the experimental BT curves and the corresponding predicted BT curves obtained for each adsorbent in Figs. 8a and 8b are similar. The adsorption capacity of BFA predicted by the Thomas model is appreciably higher than that of RHA; however, the predicted capacity of each ash is very close to its corresponding experimental capacity (q_s , Table 2). The fitting of the Thomas model for adsorption of diuron on BMA implies that external and internal diffusions are not the only rate-limiting steps [29].

3.4.4. Application of the Yoon–Nelson model

The Yoon–Nelson model is simpler than the previous models and does not involve detailed data concerning the type and properties of adsorbent, and properties of the bed [14]. The model is useful to determine the time ($t_{0.5}$) necessary for 50% saturation of column. In this study, the Yoon–Nelson model

presented by Eq. (10) is applied for the $0.01 < (C_t/C_0) < 0.97$ range and the model parameters are calculated from slope and intercept:

$$\ln\left(\frac{C_t}{C_0 - C_t}\right) = K_{YN}t - t_{0.5}K_{YN} \quad (10)$$

The kinetic constant (K_{YN} , min^{-1}) and predicted $t_{0.5}$ (min) of the Yoon–Nelson model for diuron adsorption on BMA are listed in Table 3b. The kinetic constant, K_{YN} , is increased due to driving force for mass transfer with increase in influent concentration and flow rate. A longer path that the diuron molecules travel through the bed of higher height is the reason for reduction of kinetic constant at higher bed height [32]. The BT curves predicted by the Yoon–Nelson model are compared with experimental curves in Figs. 9a and 9b for diuron adsorption on RHA and BFA, respectively. Figs. 9a and 9b indicate that the fitting of the Yoon–Nelson model is more appropriate for the diuron–BFA adsorption system than for the diuron–RHA adsorption system. This observation can be

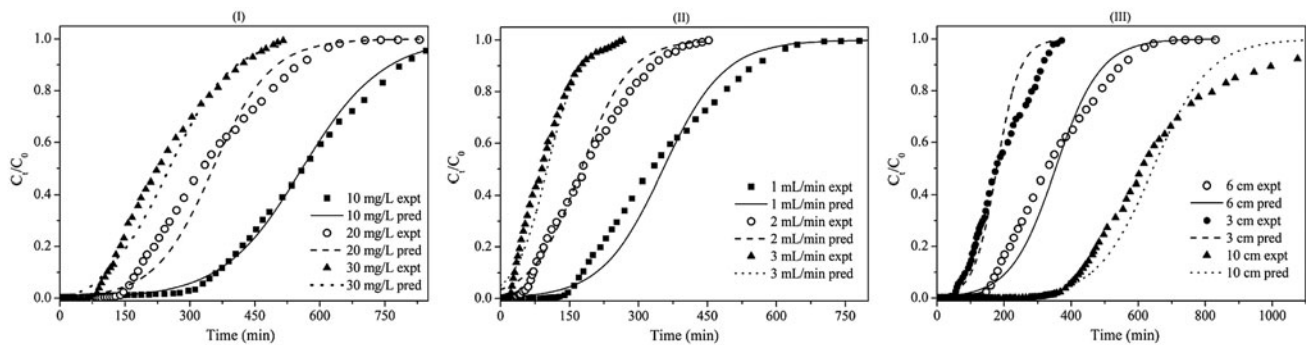


Fig. 8a. Comparison between experimental and predicted breakthrough curves for packed bed adsorption of diuron on RHA using Thomas model (I) $Q = 1$ mL/min, $Z = 6$ cm; (II) $C_0 = 20$ mg/L, $Z = 6$ cm; (III) $C_0 = 20$ mg/L, $Q = 1$ mL/min.

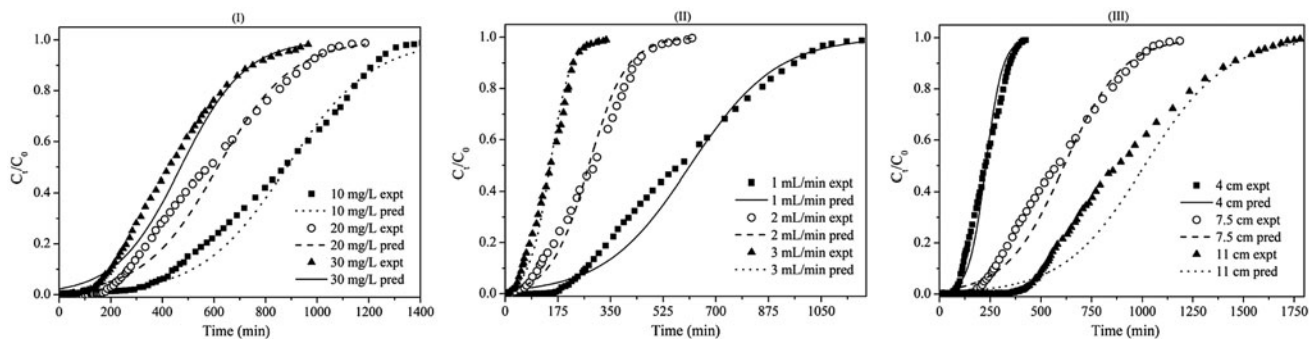


Fig. 8b. Comparison between experimental and predicted breakthrough curves for packed bed adsorption of diuron on BFA using Thomas model (I) $Q = 1$ mL/min, $Z = 7.5$ cm; (II) $C_0 = 20$ mg/L, $Z = 7.5$ cm; (III) $C_0 = 20$ mg/L, $Q = 1$ mL/min.

verified from the lower values of deviations (MPSD, ϵ) for BFA in Table 3b. Therefore, the predicted time for 50% saturation is in close accordance with the experimental time for adsorption of diuron on BFA.

3.4.5. Application of the Clark model

The Clark model is based on mass transfer coefficient and Freundlich isotherm; it is given by Eq. (11):

$$\ln\left(\left(\frac{C_0}{C_t}\right)^{n-1} - 1\right) = -rt + \ln A \quad (11)$$

The parameters, r (min^{-1}) and A for the values of (C_t/C_0) between 0.01 and 0.97 are investigated from slope and intercept and using Freundlich isotherm constant ($n = 4.4$ for RHA and 4.3 for BFA, batch study) [16]. The constants (A and r) of the Clark model for RHA and BFA are listed in Table 3b. The values of

MPSD and ϵ in Table 3b for the Clark model are large, reflecting no resemblance between experimental and predicted values. This informs the inadequacy of the Clark model for packed-bed adsorption of diuron on BMA. The Clark model is based on the ideal plug flow situation together with constant velocity of MTZ [33]. However, in this study, MTZ does not move with constant velocity, as described by the BDST model.

3.4.6. Application of deactivation kinetic model

The deactivation kinetic model [34] was initially discovered for gas–solid (packed bed) adsorption. This model is based on isothermal, pseudo-steady-state conditions and assumes negligible axial dispersion and mass transfer resistance. In addition, the model considers one active term to represent the combined effect of factors such as pore structure, active surface area, and activity per unit area of solid. The mathematical equation of the deactivation kinetic model is as follows:

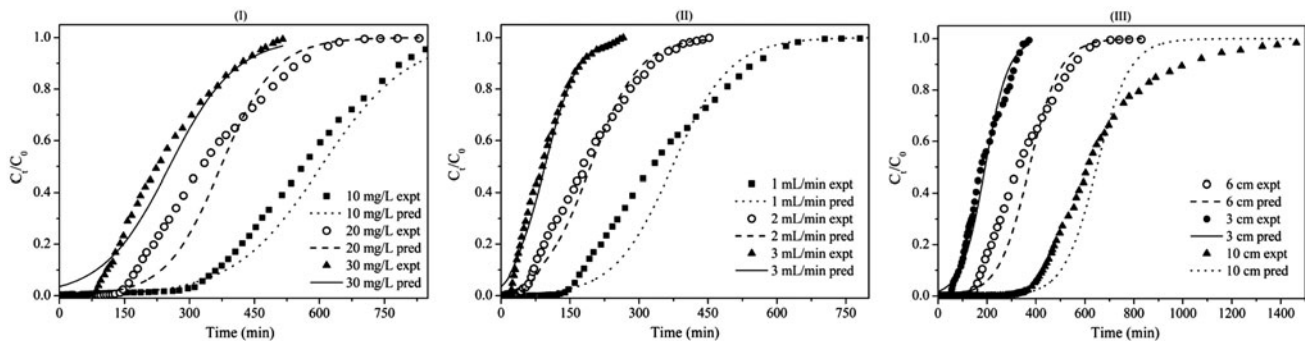


Fig. 9a. Comparison between experimental and predicted breakthrough curves for packed bed adsorption of diuron on RHA using Yoon–Nelson model (I) $Q = 1$ mL/min, $Z = 6$ cm; (II) $C_0 = 20$ mg/L, $Z = 6$ cm; (III) $C_0 = 20$ mg/L, $Q = 1$ mL/min.

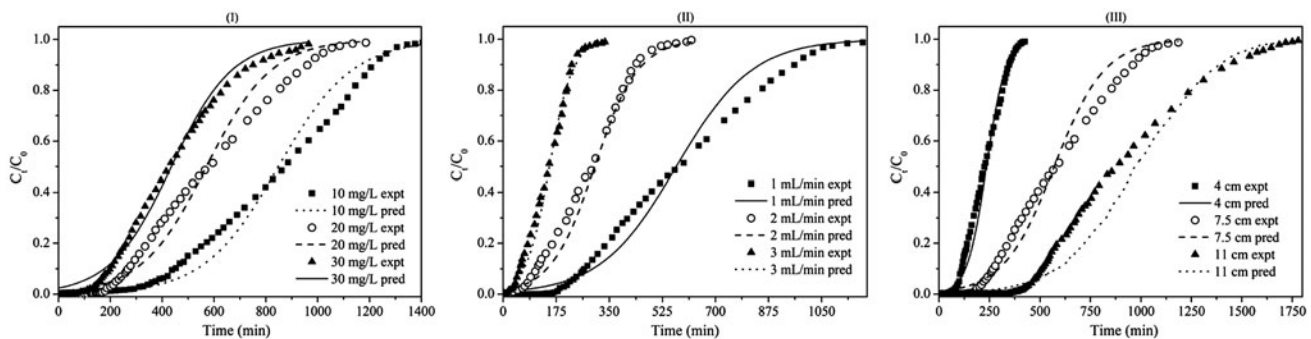


Fig. 9b. Comparison between experimental and predicted breakthrough curves for packed bed adsorption of diuron on BFA using Yoon–Nelson model (I) $Q = 1$ mL/min, $Z = 7.5$ cm; (II) $C_0 = 20$ mg/L, $Z = 7.5$ cm; (III) $C_0 = 20$ mg/L, $Q = 1$ mL/min.

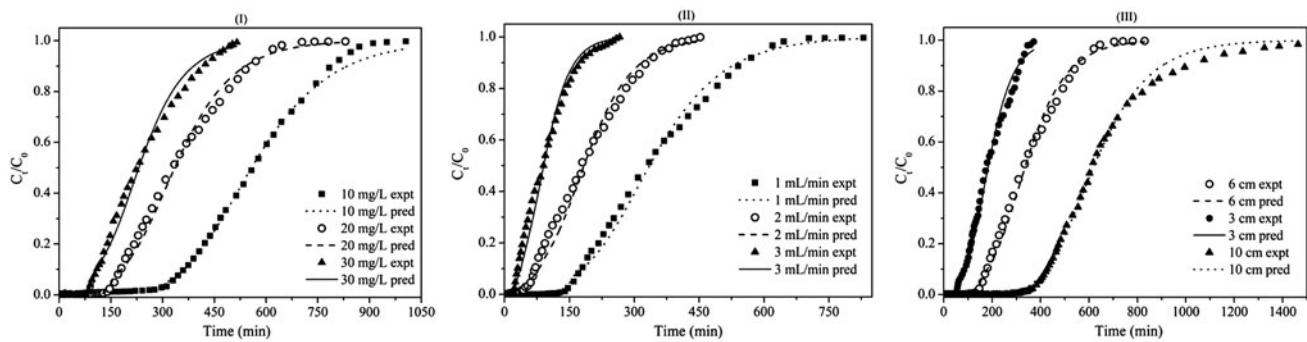


Fig. 10a. Comparison between experimental and predicted breakthrough curves for packed bed adsorption of diuron on RHA using Deactivation kinetic model (I) $Q = 1$ mL/min, $Z = 6$ cm; (II) $C_0 = 20$ mg/L, $Z = 6$ cm; (III) $C_0 = 20$ mg/L, $Q = 1$ mL/min.

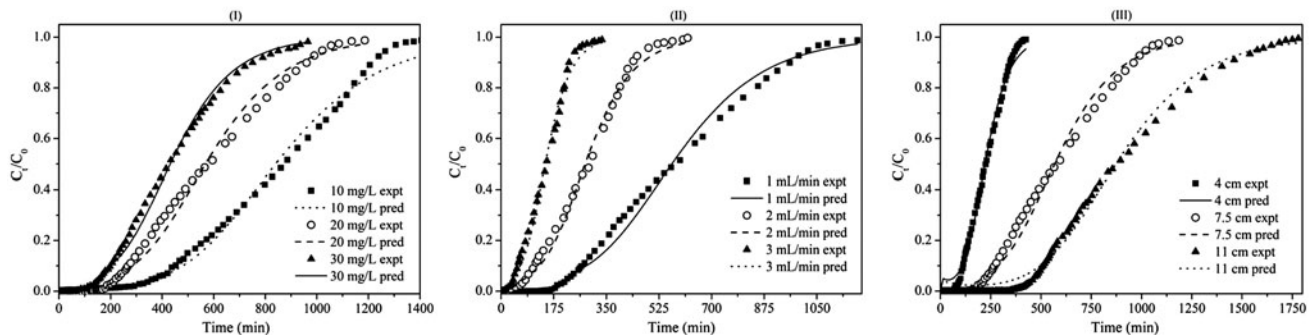


Fig. 10b. Comparison between experimental and predicted breakthrough curves for packed bed adsorption of diuron on BFA using Deactivation kinetic model (I) $Q = 1$ mL/min, $Z = 7.5$ cm; (II) $C_0 = 20$ mg/L, $Z = 7.5$ cm; (III) $C_0 = 20$ mg/L, $Q = 1$ mL/min.

$$\frac{C_t}{C_0} = \exp\left[\frac{1 - \exp(k_0 B [1 - \exp(-k_d t)])}{1 - \exp(-k_d t)} \exp(-k_d t)\right] \quad (12)$$

where $B = m/Q$ and is termed as “weight–time factor.” Eq. (12) is considered for complete saturation of RHA and BFA columns during diuron adsorption. The initial adsorption rate constant [k_0 , mL/(g min)] and deactivation rate constant (k_d , min^{-1}) are listed in Table 3b for both ashes. Figs. 10a and 10b indicate the comparison between predicted and experimental BT curves at different conditions. Among the models applied in this study, the deviation values (MPSD, ϵ) for the deactivation kinetic model are least for both RHA and BFA. Similarly, the BT curves predicted by the deactivation kinetic model are identical with experimental BT curves. Such a close approximation of BT curves is not observed for other models in this study. Thus, the deactivation kinetic model can also be proposed for solid–liquid adsorption. The present application of the deactivation model shows that the

initial adsorption rate is not much affected by influent concentration; however, the flow rate and bed height have a notable influence on adsorption rate due to the change in weight–time factor. It can be suggested from the values of k_d in Table 3b that the deactivation of BFA surface occurs slowly when compared with RHA for all experimental conditions.

4. Conclusions

The packed-bed removal of diuron using BMA is performed at different experimental conditions such as influent concentration, flow rate, and bed height. The packed-bed parameters, namely bed capacity, bed utilization, adsorbent usage rate, empty bed contact time, length of MTZ, solution treated, and breakthrough and saturation times are considerably influenced by the change in experimental parameters. The maximum bed capacity of each ash (RHA and BFA) was achieved at a higher concentration and bed height, and at a lower flow rate. The bed capacity,

volume treated, length of MTZ, adsorbent usage rate, and breakthrough and saturation times are comparatively greater for BFA than for RHA. However, bed utilization of RHA is more due to smaller MTZ.

The BDST model was applicable at 10, 50, and 90% BT of column and revealed the complex adsorption mechanism in which more than one step governs the adsorption of diuron on RHA and BFA. From the BDST model, the adsorption capacity of BFA was found to be 4,992 mg/L, whereas that of RHA was 3,052 mg/L. The Bohart–Adams and Wolborska models were found to be suitable for BFA only to describe the initial part of BT curves, whereas the Thomas model was suitable for both ashes and provides a better fitting for BT curves in the range between 0.01 and 0.97. According to the deactivation kinetic model, the BFA surface is slowly deactivated due to higher surface area, compared with RHA. The deactivation kinetic model is the best to explain the behavior of both BMA for adsorptive removal of diuron in packed bed.

Acknowledgments

We thank the Science and Engineering Research Board (SERB), India, for providing us a research grant (Grant No. SB/S3/CE/077/2013) to undertake this work. The authors thank K. Anand Kumar for substantially improving the language of this paper.

References

- [1] G.C. Chena, X.Q. Shan, Z.G. Pei, H. Wang, L.R. Zheng, J. Zhang, Y.N. Xie, Adsorption of diuron and dichlobenil on multiwalled carbon nanotubes as affected by lead, *J. Hazard. Mater.* 188 (2011) 156–163.
- [2] M.A. Bahri, L. Calvo, M.A. Gilarranz, J.J. Rodriguez, Activated carbon from grape seeds upon chemical activation with phosphoric acid: Application to the adsorption of diuron from water, *Chem. Eng. J.* 203 (2012) 348–356.
- [3] S.G. Johnston, C.T. Teppen, B.J. Boyd, Potential contribution of smectite clays and organic matter to pesticide retention in soil, *J. Agric. Food Chem.* 49 (2001) 2899–2907.
- [4] K.K. Cheung, K. Wong, C. Wong, The residual dynamic of polycyclic aromatic hydrocarbons and organochlorine pesticide in fishponds of the pearl river delta, south china, *Water Res.* 39 (2005) 1831–1843.
- [5] M.A. Fontecha-Camara, M.V. Lopez-Ramon, L.M. Pastrana-Martinez, C. Moreno-Castilla, Kinetics of diuron and amitrole adsorption from aqueous solution on activated carbons, *J. Hazard. Mater.* 156 (2008) 472–477.
- [6] Y. Liu, Z. Xu, X. Wu, W. Gui, G. Zhu, Adsorption and desorption behavior of herbicide diuron on various Chinese cultivated soils, *J. Hazard. Mater.* 178 (2010) 462–468.
- [7] J. Deng, Y. Shao, N. Gao, Y. Deng, C. Tan, S. Zhou, X. Hu, Multiwalled carbon nanotubes as adsorbents for removal of herbicide diuron from aqueous solution, *Chem. Eng. J.* 193–194 (2012) 339–347.
- [8] M.A. Bahri, L. Calvo, J. Lemus, M.A. Gilarranz, J. Palomar, J.J. Rodriguez, Mechanistic understanding of the behavior of diuron in the adsorption from water onto activated carbon, *Chem. Eng. J.* 198–199 (2012) 346–354.
- [9] G. Kyriakopoulos, D. Doulia, Adsorption of pesticides on carbonaceous and polymeric materials from aqueous solutions: A review, *Sep. Purif. Rev.* 35 (2006) 97–191.
- [10] K. Sun, Z. Zhang, B. Gao, Z. Wang, D. Xu, J. Jin, X. Liu, Adsorption of diuron, fluridone and norflurazon on single-walled and multi-walled carbon nanotubes, *Sci. Total Environ.* 439 (2012) 1–7.
- [11] J.D. Fernandez-Bayo, R. Nogales, E. Romero, Evaluation of the sorption process for imidacloprid and diuron in eight agricultural soils from southern Europe using various kinetic models, *J. Agric. Food Chem.* 56 (2008) 5266–5272.
- [12] O. Bouras, J.C. Bollinger, M. Baudu, H. Khalaf, Adsorption of diuron and its degradation products from aqueous solution by surfactant-modified pillared clays, *Appl. Clay Sci.* 37 (2007) 240–250.
- [13] R. Celis, C. Trigo, G. Facenda, M.C. Hermosin, J. Cornejo, Selective modification of clay minerals for the adsorption of herbicides widely used in olive groves, *J. Agric. Food Chem.* 77 (2007) 6650–6658.
- [14] C.B. Lopes, E. Pereira, Z. Lin, P. Pato, M. Otero, C.M. Silva, J. Rocha, A.C. Duarte, Fixed-bed removal of Hg²⁺ from contaminated water by microporous titanosilicate ETS-4: Experimental and theoretical breakthrough curves, *Microporous Mesoporous Mater.* 145 (2011) 32–40.
- [15] S.K. Deokar, S.A. Mandavgane, Estimation of packed-bed parameters and prediction of breakthrough curves for adsorptive removal of 2,4-dichlorophenoxyacetic acid using rice husk ash, *J. Environ. Chem. Eng.* 3 (2015) 1827–1836.
- [16] S.K. Deokar, D. Singh, S. Modak, S.A. Mandavgane, B.D. Kulkarni, Adsorptive removal of diuron on biomass ashes: A comparative study using rice husk ash and bagasse fly ash as adsorbents, *Desalin. Water Treat.* (in press), doi: 10.1080/19443994.2015.1132394.
- [17] Indian Standard Methods of Test for Coal and Coke, IS: 1350 (Part 1) 1984: Proximate Analysis.
- [18] V.C. Srivastava, B. Prasad, I.M. Mishra, I.D. Mall, M.M. Swamy, Prediction of breakthrough curves for sorptive removal of phenol by bagasse fly ash packed bed, *Ind. Eng. Chem. Res.* 47 (2008) 1603–1613.
- [19] S.K. Deokar, S.A. Mandavgane, B.D. Kulkarni, Behaviour of biomass multicomponent ashes as adsorbents, *Curr. Sci.* 110 (2015) 180–186.
- [20] R. Tailor, B. Shah, A. Shah, Sorptive removal of phenol by zeolitic bagasse fly ash: Equilibrium, kinetics, and column studies, *J. Chem. Eng. Data* 57 (2012) 1437–1448.
- [21] L. Vlaev, P. Petkov, A. Dimitrov, S. Genieva, Cleanup of water polluted with crude oil or diesel fuel using rice husks ash, *J. Taiwan Inst. Chem. Eng.* 42 (2011) 957–964.

- [22] V.K. Gupta, D. Mohan, S. Sharma, M. Sharma, Removal of basic dyes (Rhodamine B and Methylene Blue) from aqueous solutions using bagasse fly ash, *Sep. Sci. Technol.* 35 (2000) 2097–2113.
- [23] S.J. Kimosop, F. Orata, Z. Getenga, The influence of filter mud compost and tithoniadiversifolia leaves on the dissipation of diuron in soils within the Nzoia river drainage basin, Kenya, *Bull. Environ. Contam. Toxicol.* 89 (2012) 328–333.
- [24] R. Han, Y. Wang, W. Yu, W. Zou, J. Shi, H. Liu, Biosorption of methylene blue from aqueous solution by rice husk in a fixed-bed column, *J. Hazard. Mater.* 141 (2007) 713–718.
- [25] S. Sadaf, H.N. Bhatti, S. Ali, K. Rehman, Removal of Indosol Turquoise FBL dye from aqueous solution by bagasse, a low cost agricultural waste: Batch and column study, *Desalin. Water Treat.* 52 (2014) 184–198.
- [26] J.L. Sotelo, A. Rodríguez, S. Álvarez, J. García, Removal of caffeine and diclofenac on activated carbon in fixed bed column, *Chem. Eng. Res. Des.* 90 (2012) 967–974.
- [27] S.R. Pilli, V.V. Goud, K. Mohanty, Biosorption of Cr(VI) on immobilized *Hydrillaverticillata* in a continuous up-flow packed bed: Prediction of kinetic parameters and breakthrough curves, *Desalin. Water Treat.* 50 (2012) 115–124.
- [28] A. Jusoh, L.S. Shiung, N. Ali, M.J.M.M. Noor, A simulation study of the removal efficiency of granular activated carbon on cadmium and lead, *Desalination* 206 (2007) 9–16.
- [29] Z. Aksu, F. Gönen, Biosorption of phenol by immobilized activated sludge in a continuous packed bed: Prediction of breakthrough curves, *Process Biochem.* 39 (2004) 599–613.
- [30] M.C. Ncibi, Applicability of some statistical tools to predict optimum adsorption isotherm after linear and non-linear regression analysis, *J. Hazard. Mater.* 153 (2008) 207–212.
- [31] S. Chen, Q. Yue, B. Gao, Q. Li, X. Xu, K. Fu, Adsorption of hexavalent chromium from aqueous solution by modified corn stalk: A fixed-bed column study, *Bioresour. Technol.* 113 (2012) 114–120.
- [32] A.S.A. Aziz, L.A. Manaf, H.C. Man, N.S. Kumar, Column dynamic studies and breakthrough curve analysis for Cd(II) and Cu(II) ions adsorption onto palm oil boiler mill fly ash (POFA), *Environ. Sci. Pollut. Res.* 21 (2014) 7996–8005.
- [33] R.M. Clark, Evaluating the cost and performance of field-scale granular activated carbon systems, *Environ. Sci. Technol.* 21 (1987) 573–580.
- [34] I. Dahlan, K.T. Lee, A.H. Kamaruddin, A.R. Mohamed, Sorption of SO₂ and NO from simulated flue gas over rice husk ash (RHA)/CaO/CeO₂ sorbent: Evaluation of deactivation kinetic parameters, *J. Hazard. Mater.* 185 (2011) 1609–1613.